Hindawi
Mathematical Problems in Engineering
Volume 2018, Article ID 7070868, 19 pages
https://doi.org/10.1155/2018/7070868

Research Article

An Efficient Hybrid Approach of Finite Element Method, Artificial Neural Network-Based Multiobjective Genetic Algorithm for Computational Optimization of a Linear Compliant Mechanism of Nanoindentation Tester

Ngoc Le Chau,[1] Thanh-Phong Dao ,[2,3] and Van Thanh Tien Nguyen[1]

[1]*Faculty of Mechanical Engineering, Industrial University of Ho Chi Minh City, Ho Chi Minh City, Vietnam*
[2]*Division of Computational Mechatronics, Institute for Computational Science, Ton Duc Thang University, Ho Chi Minh City, Vietnam*
[3]*Faculty of Electrical & Electronics Engineering, Ton Duc Thang University, Ho Chi Minh City, Vietnam*

Correspondence should be addressed to Thanh-Phong Dao; daothanhphong@tdtu.edu.vn

Received 26 July 2018; Revised 26 September 2018; Accepted 4 October 2018; Published 31 October 2018

Academic Editor: Antonio Elipe

This paper proposes a new evolutionary multiobjective optimization technique for a linear compliant mechanism of nanoindentation tester. The mechanism design is inspired by the elastic deformation of flexure hinge. To improve overall static performances, a multiobjective optimization design was carried out. An efficient hybrid optimization approach of central composite design (CDD), finite element method (FEM), artificial neural network (ANN), and multiobjective genetic algorithm (MOGA) is developed to solve the optimization problem. In this procedure, the CDD is used to lay out the experimental data. The FEM is developed to retrieve the quality performances. And then, the ANN is developed as black box to call the pseudo-objective functions. Unlike previous studies on multiobjective evolutionary algorithms, most of which generating only one Pareto-optimal solution, this proposed approach can generate more than three Pareto-optimal solutions. Based on the user's real-work problem, one of the best optimal solutions is chosen. The results showed that the optimal results were found at the displacement of 330.68 μm, stress of 140.65 MPa, and safety factor of 3.6. The statistical analysis is conducted to investigate the behavior of the MOGA. The sensitivity analysis was carried out to determine the significant contribution of each factor. The results revealed that the lengths and thickness almost significantly affect both responses. It confirms that the proposed hybrid optimization approach gains high robustness and effectiveness with flexible decision maker rules to solve complex optimization engineering problems.

1. Introduction

Nanoindentation tester has attracted great interest from researchers from academics and industry. This device is now widely used in areas of material science. It is desired to probe the mechanical properties such as harness, creep, elastic-plastic modulus, and roughness surface. Materials can be tested, including hard and soft types from tissue, biological cell, nanomaterial, optics, material science, semiconductor, biomechanics, micro-electromechanical systems, and electronics [1].

During the indentation process, multiple microscopes are used to record the image of sample before and after indenting test to characterize the curve of displacement versus load. High precision positioning and stability of the system are dependent not only on the microscope, controller, and imaging technique, but also a mechanical-driven platform. The platform is utilized to bring the material in front of microscope and then a picture is taken. And then, the platform takes the material to the location of indenter so as to do an indentation. At last, the platform brings the material to return back the location of microscope to characterize the curve of displacement versus load. It can be concluded that the mechanical-driven platform is a critical mechanism for the nanoindentation tester. In commercialization, the current instruments are relatively effective but so costly. The reason

is that, in the current nanoindentation tester system, a ball-screw driven system by servo motors or linear motors is used to ensure the linear precision. However, such mechanical-driven systems possess some common defects such as assembly gap, wear and aging, and friction error, which may restrict their further applications in the nanoindentation industries where micro or nanoscale positioning accuracy is needed. Hence, it has been a difficult challenge for researchers to make a cheaper system with better accuracy.

To eliminate the cost and enhance the positioning accuracy, a linear compliant mechanism (LCM) is proposed in this study to bring the observed material. The proposed LCM is operated based on ideal of elastic springs and has no backlash, free friction, high precision, and monolithic structure [2–5]. Meanwhile, the servo-driven system causes large backlash and friction between kinematic joints. To create more precise and light positioning system, the LCM is recommended as a potential candidate. There have not been studies on the LCM for positioning the material in nanoindentation tester yet. LCM is now used to handle displacement from a few micrometers to hundreds of micrometers. The proposed LCM can meet a good precision positioning but its workspace and life time are limited because its operation relies on elastic links. In addition, the common piezoelectric actuator-guided nanopositioning stages have the problems of small travel range because the piezoelectric actuator has a limited travel range of less than 200 μm.

To meet the practice requirements of advanced material sciences, the capability of a large positioning space and long working life of the LCM should be improved further. To overcome the limitation of performances, common procedures are, for example, topology and size optimization. Topology represents the connectivity of the domain. Size optimization denotes design parameters such as thickness, cross-sectional area, and length [6–8]. Shape optimization represents a suitable configuration. In general, mathematical equations are often established, and then an evolutionary optimization algorithm is used to seek a set of optimal design parameters [9]. If the established mathematical equations are not right, the optimized results will not be accurate.

For these reasons, this study introduces a new evolutionary multiobjective optimization technique for optimizing the performances of LCM to decrease the modeling errors. The proposed optimization approach is a hybrid intelligent integration of central composite design (CDD), finite element method (FEM), artificial neural network (ANN), and multiobjective genetic algorithm (MOGA). Each of the mentioned methods has been used widely but individually. For example, CDD was investigated in building and optimizing [10–15], FEM was used in various engineering fields [9, 16–18], ANN was employed for thermal or other engineering disciplines [19–23], and MOGA was utilized for optimizing multiple responses [24–26]. Although these methods were well known, hybridization of them has not been developed for optimization of the LCM. Therefore, an integration of hybrid optimization approach is a main purpose of this study. In addition, most of previous multiobjective evolutionary algorithms (MOEAs) often give a Pareto-optimal front. Unlike previous MOEAs, the proposed hybrid algorithm can generate more number of optimal solutions. This helps users choose the best solution for real-work purpose.

The computationally evolutionary optimization approach is developed to satisfy a tradeoff between performance characteristics of LCM. In this hybrid optimization approach, a model is created via using finite element method. Subsequently, based on central composite design (CCD), a number of simulated experiments are generated and the results of performances are automatically generated via FEM. And then, relationship between design parameters and output performances will be generated well by using the ANN technique. ANN is as a black box to map well the inputs and outputs. Finally, MOGA is integrated to seek an optimal solution. This optimization process is totally automatic solution to gain accurate results.

The purposes of this paper are to propose an optimal design strategy for the LCM in terms of good static characteristics. Elastic joints of the LCM are designed based on elastic springs. A lever-displacement amplifier is used to amplify the workspace. To improve the static performances, a hybrid optimization algorithm is developed. A validation is performed to evaluate predicted results, efficiency, and robustness of the proposed approach.

2. Design of Linear Compliant Mechanism

2.1. Compliant Displacement Amplification. Although the piezoelectric stack actuator (PSA) was a common actuator for precision positioning platform and manipulator, it is still limited by its working travel. To overcome this limitation, the lever-displacement amplification is often used to amplify the travel of PSA.

A traditional lever-displacement amplifier is depicted, as seen in Figure 1(a). The length of lever is divided into two parts with input distance L_1 and output distance L_o. Figure 1(b) illustrates the kinematic diagram for operation principle. When the input load is exerted at the input port, point A moves to A'. At the same time, the output port is moved from point B to B'. The vertical link serves as elastic joint or flexure hinge.

The traditional amplification ratio can be calculated as follows:

$$R = \frac{L_o}{L_i} = \frac{\delta_2}{\delta_1}, \tag{1}$$

in which, δ_1 and δ_2 are the input displacement and output displacement, respectively.

In the field of precision positioning system, compliant mechanisms (CMs) are operated relying on the elastic deformation of thin cross section links [27]. CMs are largely dependent on the lump or distributed elastic elements. These elastic parts work under the yield strength while the deformation of flexure hinges is eliminated. Hence, a compliant displacement amplification (CDA) mechanism with two levers was proposed in this study. The CDA included a lever in the left and another lever in the right. The CDA was intended to amplify the work travel of linear compliant mechanism (LCM). As seen in Figures 2(a) and 2(b), when a

Table 1: Properties of material Al 7075.

Material properties			
Density	Poison's ratio	Young's modulus	Yield strength
2810 kg/m^3	0.33	71.70 GPa	503 MPa
Parameters	Unit	Dimension	
$t_1, t_2, t_3, l_1, l_2, l_3$	mm	Variables	

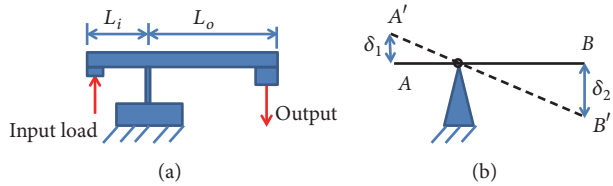

Figure 1: Traditional lever-displacement amplification: (a) model, (b) kinematics.

force was applied at the input port of the CDA, the movement of the output port of CDA was amplified.

The basic mathematical model for the CDA was computed as follows:

$$R_{new} = n \times \frac{L_o}{L_i} = n \times \frac{\delta_2}{\delta_1}, \quad (2)$$

in which, n is the number of used levers.

As seen in (2), the amplification ratio of CDA was n times the traditional amplification ratio in (1).

As depicted in Figure 2, the LCM was only desired to move along the y-axis. The links with thickness t_1 and length l_1 served as flexure hinge and helped to eliminate the parasitic motion along the x-axis. Other links with thicknesses t_2 and t_3 and lengths l_2 and l_3 were geometrical parameters of CDA. The LCM had width of w. Overall design parameters were the most important parameters affecting the performances of the precision positioning system. The Al 7075 was selected as material for the LCM. The parameters of material and design parameters were given, as in Table 1.

2.2. Primary Application for Nanoindentation Tester. In the material field, inspecting mechanical properties of a soft and thin material sample during nanoindentation test is critical work. Figure 3 illustrates a potential application of the LCM for nanoindentation tester. It includes 5 important parts with different functions. The top plate was connected with the base to serve as fixed stationary. A microscope was fixed on the top plate so as to monitor the material sample. The LCM was used to bring the material sample. At the beginning, the sample was pictured by the microscope. The microscope was used to drive a microscope/lens so as to observe the prior-and-later surface of material. And then, the imaged pictures are analyzed using image technique. As a result, the mechanical properties can be extracted from the curve of load-displacement and this type of curve should ensure accurately. And then, the sample was moved to a location of the indenter. At last, the indenter would indent inside the sample and at the same time the microscope would defect the indentation depth and specifications of the deformed sample.

3. Formulation of Multiobjective Optimization Problem

Existing nanoindentation tester has attracted a great interest in material engineering. It is used for various materials such as biological tissues and soft gels. Commercialized instruments can monitor easily the mechanical properties of a sample but its operating costs are rather high. A high cost may come from positioning system where motors and actuators are utilized simultaneously. To fulfill higher precise probe requirements in several tens of micrometers to hundreds of millimeters, the proposed LCM was used to decrease the motors and actuators. Hence, the considerable challenges have been faced when developing the nanoindentation devices; the instruments should have the following specifications: (i) able to give a large displacement; (ii) able to speed up the indentation process; (iii) able to ensure a long working time; (iv) able to gain an excellent stability; and (v) able to record the displacement and force signal itself before and after indentation process.

Specifically, the LCM could give a large displacement and a long working time for nanoindentation tester. In this system, the LCM should fulfill the following important requirements: to satisfy faced challenges as

(a) a large working stroke to allow suitability for various materials;

(b) a high safety factor to enhance the fatigue life.

In general, these requirements conflicted together. A tradeoff multiple responses could be gained by developing a new hybrid optimization approach.

3.1. Design Variables. It was noted that the proposed LCM was very sensitive to geometric dimensions such as thicknesses, lengths, and width. Therefore, these parameters were considered as the design variables. The vector of design variables was set as $\mathbf{X} = [t_1, t_2, t_3, l_1, l_2, l_3, w]^T$.

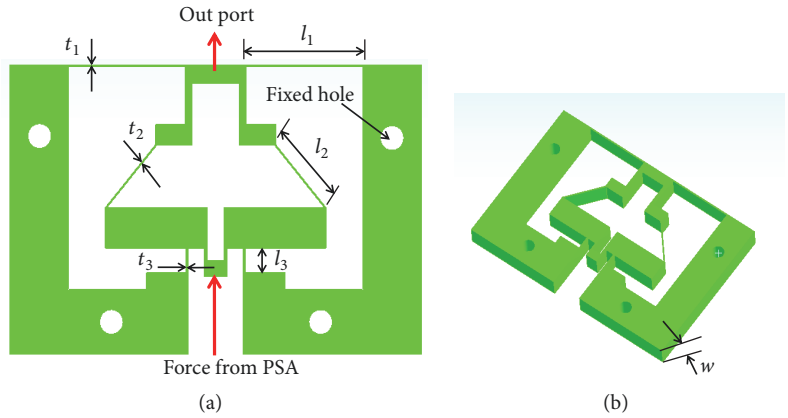

Figure 2: Linear compliant mechanism: (a) 2D diagram, (b) 3D model.

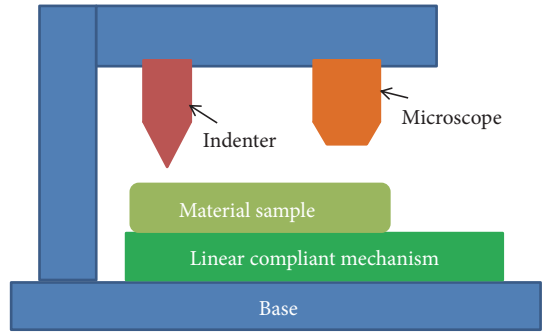

Figure 3: 2D model of a nanoindentation tester.

The lower and upper bounds for the design variables were assigned as follows:

$$\begin{aligned} 0.45\,\text{mm} &\le t_1 \le 0.55\,\text{mm} \\ 0.36\,\text{mm} &\le t_2 \le 0.44\,\text{mm} \\ 0.45\,\text{mm} &\le t_3 \le 0.55\,\text{mm} \\ 27\,\text{mm} &\le l_1 \le 33\,\text{mm} \\ 18\,\text{mm} &\le l_2 \le 22\,\text{mm} \\ 5.4\,\text{mm} &\le l_3 \le 6.6\,\text{mm} \\ 5\,\text{mm} &\le w \le 15\,\text{mm}, \end{aligned} \tag{3}$$

where t represents the thickness of flexure hinges, l_i represents length of ith flexure hinge with $i = [1, 2, 3]$, and w is the width of LCM.

3.2. Objective Functions. The multiple quality performances of LCM were as follows: (i) the displacement, $f_1(\mathbf{X})$, was desired as large as possible; (ii) the safety factor, $f_2(\mathbf{X})$, is required as high as possible. To summarize, the optimization problem was briefly stated as follows:

$$\max f_1(\mathbf{X}), \tag{4}$$

$$\max f_2(\mathbf{X}). \tag{5}$$

3.3. Constraints. The resulting stress of the LCM must be under the yield strength of the material, which was described as follows:

$$g(\mathbf{X}) \le \frac{\sigma_y}{f_2(\mathbf{X})}, \tag{6}$$

where $g(\mathbf{X})$is the resulting stress and σ_y is the yield strength of proposed material s.t.

$$f_1(\mathbf{X})_{\max} \ge 300\,\mu\text{m}, \tag{7}$$

$$f_2(\mathbf{X})_{\min} \ge 3. \tag{8}$$

4. Hybrid Optimization Algorithm

Before conducting an engineering optimization problem, mathematical models are traditionally established, and then a suitable optimization algorithm is utilized. The fact is that there would be an error between mathematical models and simulations or experiments. This is because those models may not be right and depend mainly on capability and knowledge of researchers about engineering and mathematical theory. Therefore, an evolution optimization algorithm can then generate inaccurate results. To overcome this limitation, a hybrid approach of RSM, FEM, ANN, and MOGA was proposed in this study so as to improve the quality performances of the LCM. The robustness and efficiency of

proposed approach could be validated through simulated experiments. Figure 4 illustrates a systematic flowchart for the multiobjective optimization procedure. The optimization process was carried out by three large phases and substeps as follows.

Phase 1 (computer aid engineering application and design). Nowadays, with a fast development of computer, a high performance computer (HPC) can perform a thousands of calculations per a second, which is considered as a workstation. Based on these advantages, machine learning and artificial intelligent algorithms can be programed well to meet a research and development in engineering. It can be called computer aid engineering application and design (CAD A&D). The first stage to optimize the CDA, a CAD A&D process for the CDA, was conducted by following steps.

Step 1 (define problem). The CDA was deigned to serve as a displacement amplifier for applications in precision engineering micro- or nanopositioning systems. In these devices, a piezo stack actuator (PSA) serves as an actuator but its travel is limited. Therefore, the CDA was intended to amplify the work travel for PSA, a product from Physik Instrumente Co., Ltd. Multiobjective optimization problem for the CDA was conducted to improve its quality performances.

Step 2 (mechanical structure). A mechanical structure was proposed based on designer's experience and perception. Initially, many drafts were drawn to illustrate the highlights of CDA. A final model was chosen but its specifications cannot meet the requirements of positioning system.

Step 3 (define design variables and objective functions). The lengths and thicknesses of flexure hinge and the width of the CDA were determined as design variables. The reason was that these parameters affect the performances of the CDA. These variables can be seen as Figure 1.

To meet the practical requirements of customers, a precision positioning system must have a large workspace, a high speed, a high safety factor, and a minimum stress. All these performances can be fulfilled by optimizing the CDA because the mechanical structure and geometries of CDA contribute to the system. Hence, the mentioned quality characteristics were taken into account as four objective functions.

Step 4 (build 3D model). A 3D model was drawn by using FEM. The FEM is a computational technique used to obtain approximate solutions of problems in engineering. Postprocessor contains sophisticated routines used for sorting, printing, and plotting selected results from a finite element solution. Because the CDA was an elastic structure, during the analysis some of the following relationships were used.

According to the linear Hooke's law, the equation describing a relation between the force and displacement was computed as

$$\mathbf{F} = \mathbf{KU}, \tag{9}$$

where $\mathbf{K}$ is the global stiffness matrix that is computed according to finite element principle. Correspondingly, the global displacement vector $\mathbf{U}$ and force vector $\mathbf{F}$ for all nodes can be calculated as

$$\mathbf{U} = \left[\left(\mathbf{q}^1\right)^{\mathrm{T}}, \ldots, \left(\mathbf{q}^i\right)^{\mathrm{T}}, \left(\mathbf{q}^n\right)^{\mathrm{T}}\right]^{\mathrm{T}}, \tag{10}$$

$$\mathbf{F} = \left[\left(\mathbf{F}^1\right)^{\mathrm{T}}, \ldots, \left(\mathbf{F}^i\right)^{\mathrm{T}}, \left(\mathbf{F}^n\right)^{\mathrm{T}}\right]^{\mathrm{T}}, \tag{11}$$

where n is the total number of nodes and $\mathbf{q}^i$ and $\mathbf{F}^i$ are the displacement and force vectors of node i, which can be determined by

$$\mathbf{q}^i = \left[u_x^i, u_y^i, \theta_z^i\right], \quad i = 1, 2, \ldots, \mathrm{n} \tag{12}$$

$$\mathbf{F}^i = \left[F_x^i, F_y^i, M_z^i\right], \quad i = 1, 2, \ldots, \mathrm{n} \tag{13}$$

where u_x^i and u_y^i are the displacement along the x- and y-axes of node ith. θ_z^i is the rotational angle of node ith. F_x^i and F_y^i are applied forces and M_z^i is moment.

Also by Hooke's law, the relationship between stress and strain was calculated as follows:

$$\sigma = E\varepsilon, \tag{14}$$

where σ, E, ε are the stress and Young's modulus, sequentially.

Step 5 (evaluate initial performances). The 3D model was drawn in Step 4 and considered as a draft design. It had four quality performances, as given in Step 3; namely, a precision positioning system must have a large workspace, a high speed, a high safety factor, and a minimum stress. Such performances should be evaluated by implementing FEM simulations. This step ended the CAD A&D process. If the CDA's specifications were not satisfied according to the designer's requirements, the process would return to Step 2. If it was ok, it would move to Phase 2.

Phase 2 (response surface and regression model). Prior to optimization process, virtually pseudo-mathematical equations could be treated as fitness functions. To do this, a number of experiments were generated and simulated data were collected. At last, the regression models were established to map design variables and outcome performances.

Step 6 (design of experiment). By using the RSM-integrated FEM, a numbers of simulation experiments were planned via using the central composite design integrated with RSM. The number of necessary experiments was determined by the following equation:

$$N = 2^{(k-f)} + 2k + n_c, \tag{15}$$

where N was the total of the design points, k was the number of design variables, f was the factorial number ($f = 0$), and $n_c = 1$ was the number of replicates at the center point of the design space.

Step 7 (generate data). The simulated experimentations were collected based on an integration of RSM and FEM. First,

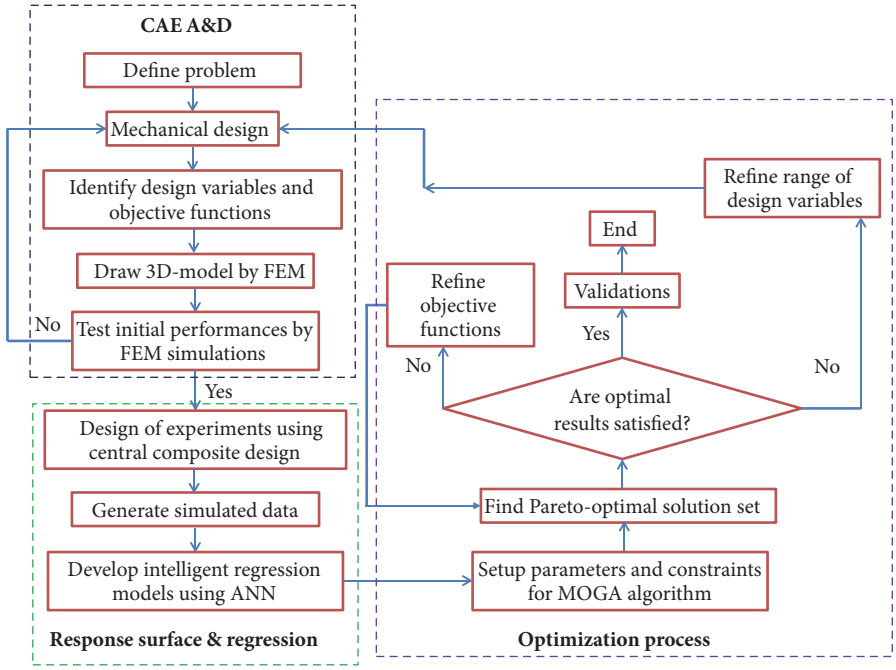

Figure 4: The flowchart of hybrid optimization procedure.

they were based on the 3D model designed in the FEM in the Step 4. Subsequently, the estimated results for the quality responses were retrieved based on finite element analysis (FEA).

Step 8 (establish regression models). There were various regression models such as full 2nd-order polynomials, artificial neural network, and nonparametric regression. In this study, ANN was a suitable candidate for the retrieved data. It was used as a regression approach for the estimated database. It was considered as a black box to approximate the complex nonlinear relationship between design parameters and the qualities. ANN model can find a pseudo-objective functions. These objective functions were used for the MOGA algorithm.

Phase 3 (operation of MOGA). After the pseudo-objective functions were determined in Step 8, the optimization process was implemented by setup controllable parameter and programing MOGA algorithm. This algorithm was proposed for multiobjective optimization problem in this study because it can converge to the global Pareto solutions. This algorithm was used to seek a Pareto-optimal set for multiobjective optimization problem. A flowchart of proposed MOGA procedure was illustrated in Figure 5.

Step 9 (initialize controllable parameters of MOGA). The multiobjective genetic algorithm (MOGA) was a variant of the nondominated sorted genetic algorithm-II (NSGA-II) that relied on controlled elitism concepts. It can solve multiple objectives and constraints. At last, the MOGA can find the global optimum solution. The controllable parameters of MOGA in this study were given in Table 2. This algorithm includes some important parameters such as population size, crossover probability, mutationprobability, and number of generations. To achieve an accurate optimal solution, correct selection of the parameters (crossover, mutation, size of population, and number of generations) would be conducted later. Table 2 gives the range of tuning parameters of the MOGA.

Table 2: Controllable parameters for MOGA algorithm.

Parameters	Range of value
Population size	20-100
Number of generations	50-150
Crossover probability	0.2-0.9
Mutation probability	0.01-0.02
Maximum number candidates	3

Step 10 (computing the fitness value). This step was critical to change the fitness so as to gain the fitness values of the individuals.

Step 11 (selection operator). The usual selection operator, such as Monte Carlo, was used and combined with the elitist model.

Step 12 (crossover operator). Crossover operation was utilized to produce parent generation.

Step 13 (mutation operation). Mutation operation was used to generate new generation.

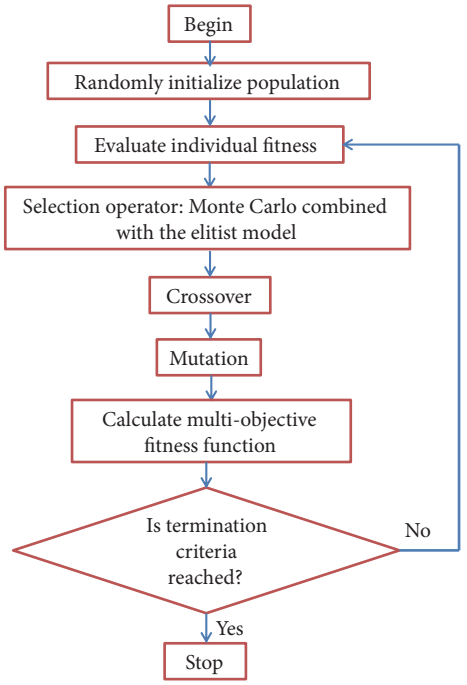

Figure 5: Flowchart of MOGA algorithm.

Step 14 (termination criteria). If the gross generation was gained and the best individual was found through predetermined iterations, the MOGA was stopped. Otherwise, Step 10 was repeated.

Phase 4 (evaluate optimum candidates). The best candidates were found by using MOGA and then the final phase was overall evaluations of these candidates.

Step 15 (find the Pareto-optimal set). Multiobjective optimization problem was solved by using MOGA, and then the tradeoff the objective optimizations was treated as Pareto-optimal set. At last, the optimal results were found.

Step 16 (evaluate optimal candidates). If the optimal results were satisfying, the extra validations were conducted to evaluate the robustness and efficiency of the proposed hybrid optimization approach. The optimization process was ended herein. If they were not well refined, the optimization process would be further enhanced by Step 17 or Step 18.

Step 17 (refine objective functions). In performing the optimization process, a refinement was the most important phase to seek the optimal solutions. After optimal candidates were generated and based on the initial requirements of quality characteristics, the researchers would evaluate the candidates. If there was no candidate that was satisfying, the ranges of quality characteristics or the range of design variables must be controlled or refined again from Step 15. This step was repeated until the best candidate was found.

Step 18 (refine range of design variables). If Step 13 was not well turned, the optimization process would act on the range of design variables. The ranges could be increased or decreased. Steps 2–12 were repeated. Otherwise, Step 13 would be repeated.

Table 3: Initial parameters and performances.

Design parameter	Initial design	Unit
t_1	0.5	mm
t_2	0.4	mm
t_3	0.5	mm
l_1	30	mm
l_2	20	mm
l_3	6	mm
w	10	mm
Displacement	295.59	μm
Safety factor	2.7331	

5. Results and Discussion

5.1. Test Initial Performances. A 3D model was created in FEM design modeler, and then FEA simulations were conducted to test the initial performance of LCM. As shown in Table 3. The results showed that the displacement is about 295.59 μm and safety factor is approximately 2.733. The two values are not satisfying for the desired requirements by constraints in (7)-(8). Therefore, to meet the used actual requirement of nanoindentation tester, the two characteristics should be further optimized.

5.2. Experimental Data. As proposed hybrid optimization approach, a 3D model of the LCM was designed via using

Table 4: Design of experiments and training data using CCD.

No.	l_1 (mm)	t_1 (mm)	l_2 (mm)	t_2 (mm)	l_3 (mm)	t_3 (mm)	w (mm)	Displacement (μm)	Safety factor
1	30	0.5	20	0.4	0.5	6	10	472.59	3.63
2	30	0.5	20	0.4	0.5	6	5	476.33	3.68
3	30	0.5	20	0.4	0.5	6	15	474.79	3.57
4	30	0.5	18	0.4	0.5	6	10	602.70	1.87
5	30	0.5	22	0.4	0.5	6	10	392.22	2.61
6	30	0.5	20	0.36	0.5	6	10	481.24	3.62
7	30	0.5	20	0.44	0.5	6	10	467.73	3.77
8	30	0.5	20	0.4	0.45	6	10	468.62	3.72
9	30	0.5	20	0.4	0.55	6	10	475.77	3.68
10	30	0.5	20	0.4	0.5	5.4	10	473.37	3.60
11	30	0.5	20	0.4	0.5	6.6	10	471.30	3.67
12	27	0.5	20	0.4	0.5	6	10	465.98	3.74
13	33	0.5	20	0.4	0.5	6	10	478.28	3.66
14	30	0.45	20	0.4	0.5	6	10	473.23	3.64
15	30	0.55	20	0.4	0.5	6	10	470.26	3.71
16	28.93	0.51	19.29	0.38	0.48	5.78	8.23	521.26	2.94
17	28.93	0.48	19.29	0.38	0.48	5.78	11.76	524.74	3.04
18	28.93	0.48	20.70	0.38	0.48	5.78	8.23	431.56	3.36
19	28.93	0.51	20.70	0.38	0.48	5.78	11.76	434.51	3.78
20	28.93	0.48	19.29	0.41	0.48	5.78	8.23	515.78	3.01
21	28.93	0.51	19.29	0.41	0.48	5.78	11.76	514.26	3.12
22	28.93	0.51	20.70	0.41	0.48	5.78	8.23	428.35	3.35
23	28.93	0.48	20.70	0.41	0.482	5.78	11.76	432.74	3.78
24	28.93	0.48	19.29	0.38	0.51	5.78	8.23	527.63	2.88
25	28.93	0.51	19.29	0.38	0.51	5.78	11.76	526.40	3.03
26	28.93	0.51	20.70	0.38	0.51	5.78	8.23	438.24	3.53
27	28.93	0.48	20.70	0.38	0.51	5.78	11.76	436.99	3.76
28	28.93	0.51	19.29	0.41	0.51	5.78	8.23	517.02	2.97
29	28.93	0.48	19.29	0.41	0.51	5.78	11.76	520.74	3.04
30	28.93	0.48	20.70	0.41	0.51	5.78	8.23	434.69	3.49
31	28.93	0.51	20.70	0.41	0.51	5.78	11.76	431.84	3.71
32	28.93	0.48	19.29	0.38	0.48	6.21	8.23	522.59	3.00
33	28.93	0.51	19.29	0.38	0.48	6.21	11.76	524.15	3.05
34	28.93	0.51	20.70	0.38	0.48	6.21	8.23	430.91	3.42
35	28.93	0.48	20.70	0.38	0.48	6.21	11.76	434.53	3.96
36	28.93	0.51	19.29	0.41	0.48	6.21	8.23	512.86	3.07
37	28.93	0.48	19.29	0.41	0.48	6.21	11.76	513.27	3.12
38	28.93	0.48	20.70	0.41	0.48	6.21	8.23	433.47	3.44
39	28.93	0.51	20.70	0.41	0.48	6.21	11.76	430.08	3.89
40	28.93	0.51	19.29	0.38	0.51	6.21	8.23	523.21	2.93
41	28.93	0.48	19.29	0.38	0.51	6.21	11.76	526.51	3.04
42	28.93	0.48	20.70	0.38	0.51	6.21	8.23	438.89	3.67
43	28.93	0.51	20.70	0.38	0.51	6.21	11.76	437.81	3.79
44	28.93	0.48	19.29	0.41	0.51	6.21	8.23	517.41	2.99
45	28.93	0.51	19.29	0.41	0.51	6.21	11.76	514.68	3.06
46	28.93	0.51	20.70	0.41	0.51	6.21	8.23	433.78	3.33
47	28.93	0.48	20.70	0.41	0.51	6.21	11.76	433.24	3.74

Table 4: Continued.

No.	l_1 (mm)	t_1 (mm)	l_2 (mm)	t_2 (mm)	l_3 (mm)	t_3 (mm)	w (mm)	Displacement (μm)	Safety factor
48	31.06	0.48	19.29	0.38	0.48	5.78	8.23	529.57	2.93
49	31.06	0.51	19.29	0.38	0.48	5.78	11.76	527.76	3.06
50	31.06	0.51	20.70	0.38	0.48	5.78	8.23	441.45	3.60
51	31.06	0.48	20.70	0.38	0.48	5.78	11.76	440.86	3.82
52	31.06	0.51	19.29	0.41	0.48	5.78	8.23	520.39	2.99
53	31.06	0.48	19.29	0.41	0.48	5.78	11.76	522.99	3.09
54	31.06	0.48	20.70	0.41	0.48	5.78	8.23	438.41	3.54
55	31.06	0.51	20.70	0.41	0.48	5.78	11.76	436.12	3.65
56	31.06	0.51	19.29	0.38	0.51	5.78	8.23	530.31	2.94
57	31.06	0.48	19.29	0.38	0.51	5.78	11.76	533.15	3.01
58	31.06	0.48	20.70	0.38	0.51	5.78	8.23	439.53	3.32
59	31.06	0.51	20.70	0.38	0.51	5.78	11.76	444.13	3.78
60	31.06	0.48	19.29	0.41	0.51	5.78	8.23	524.97	2.94
61	31.06	0.517	19.29	0.41	0.51	5.78	11.76	524.10	3.05
62	31.06	0.51	20.70	0.41	0.51	5.78	8.23	435.03	3.32
63	31.06	0.48	20.70	0.41	0.51	5.78	11.76	439.34	3.72
64	31.06	0.51	19.29	0.38	0.48	6.21	8.23	526.08	3.01
65	31.06	0.48	19.29	0.38	0.48	6.21	11.76	529.12	3.05
66	31.06	0.48	20.70	0.38	0.48	6.21	8.23	436.64	3.44
67	31.06	0.51	20.70	0.38	0.48	6.21	11.76	440.67	3.84
68	31.06	0.48	19.29	0.41	0.48	6.21	8.23	520.62	2.99
69	31.06	0.51	19.29	0.41	0.48	6.21	11.76	520.96	3.13
70	31.06	0.51	20.70	0.41	0.48	6.21	8.23	436.90	3.41
71	31.06	0.48	20.70	0.41	0.48	6.21	11.76	438.74	3.86
72	31.06	0.48	19.29	0.38	0.51	6.21	8.23	530.51	2.92
73	31.06	0.51	19.29	0.38	0.51	6.21	11.76	527.16	3.03
74	31.06	0.51	20.70	0.38	0.51	6.21	8.23	442.88	3.63
75	31.06	0.48	20.70	0.38	0.51	6.21	11.76	442.26	3.88
76	31.06	0.51	19.29	0.41	0.51	6.21	8.23	521.42	3.04
77	31.06	0.48	19.29	0.41	0.51	6.21	11.76	522.38	3.07
78	31.06	0.48	20.70	0.41	0.51	6.21	8.23	434.91	3.32
79	31.06	0.51	20.70	0.41	0.51	6.21	11.76	439.50	3.56

FEM. With six design variables, the numbers of experiments were calculated using the central composite design in (15).

And then, based on Kriging regression model, each pseudo-objective function was made for the displacement, resulting stress, and safety factor. Finally, by integrating FEM, RSM, and ANN regression model, the real values of three quality responses were automatically computed, as given in Table 4.

5.3. Regression Model. Compared with other regression models such as full 2nd-order polynomials, nonparametric regression, and Kriging model, artificial neural network gave relatively correct results. The coefficient of determination of ANN model was approximately 1, as given in Table 5. This value was relatively well for a regression model. It was considered as a performance criterion. To sum up, the built ANN can be regarded as the pseudo-objective functions that described the relation between design parameters and the displacement and safety factor. The data from the table was randomly divided into training of 70% of data, validation of 15% of data, and testing of 15% of data.

The structure of an ANN was determined by the number of layers, the number of nodes in each layer, and the nature of the transfer functions. This paper used three-layered feed forward back propagation neural network (7:10:1), as shown in Figure 6.

In this study, the Bayesian Regularization was chosen as the training method for the safety factor data because it permitted a coefficient of determination (R^2) of approximately 1. Meanwhile, to gain the R^2 of 1, the Levenberg-Marquardt was suitable for the displacement data. Training, validation, and testing all had a mean square error of about zero, as

Table 5: Goodness of fit of regression models.

Artificial neural network model		
Performance criteria	Displacement	Safety factor
Coefficient of determination	1	1
Mean square error	0	0

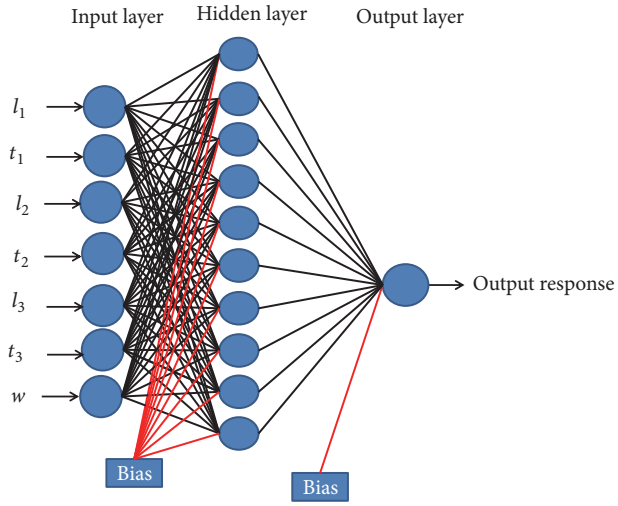

Figure 6: Structure of the developed ANN.

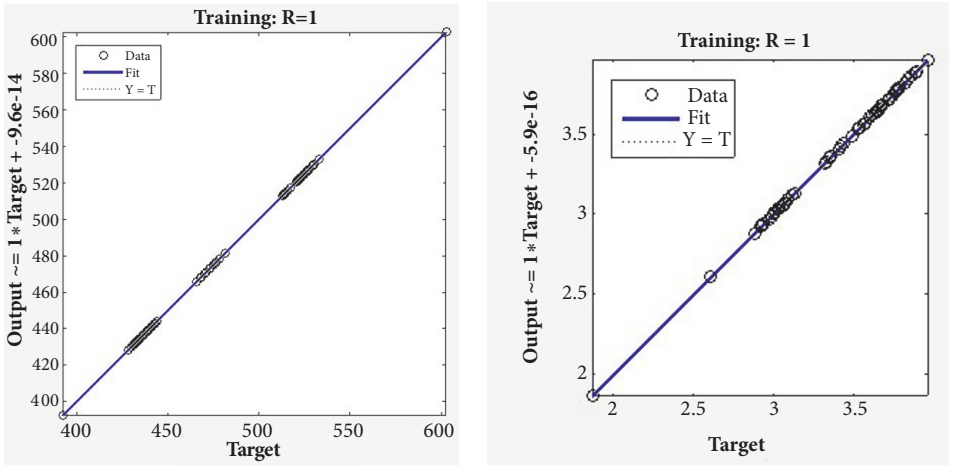

(a) (b)

Figure 7: Regression plots: (a) the displacement and (b) safety factor.

shown in Figure 7 and Table 5. The results showed that the performances of the proposed ANN models are good for the data.

The contribution of each parameter and interaction affecting the displacement was analyzed in Table 6. The results showed that the length l_2 has a largest contribution of 97.78% with respect to the displacement and statistical significance with p-value of 0.000 (less than 0.05%).

As shown in Table 7, the length l_2 also had a largest contribution on the safety factor with 50.14% and a good statistical significance with p-value of 0.000 (less than 0.05%).

5.4. Optimal Results. By using Phase 3 and begining from Step 5, MOGA was integrated with FEM, RSM, and ANN to seek a tradeoff between the displacement and safety factor. During the optimization process, the optimal results were generated automatically. Many of potential candidates would be retrieved but some might not good and could not find any value. Therefore, this study proposed two ways to gain the candidates. The first way was an adjustment on the range of design parameters. The second way was a change in the range of objective functions. After implementing many optimization processes to conduct and prove the two

Table 6: Response surface regression of displacement versus design parameters.

Source	DF	Seq SS	Contribution	Adj SS	Adj MS	F-Value	P-Value
Model	35	143821	99.61%	143821	4109	316.88	0.000
Linear	7	142517	98.71%	110807	15830	1220.71	0.000
l_1	1	548	0.38%	436	436	33.63	0.000
t_1	1	17	0.01%	39	39	2.99	0.091
l_2	1	141172	97.78%	109802	109802	8467.46	0.000
t_2	1	657	0.46%	454	454	34.99	0.000
l_3	1	102	0.07%	56	56	4.35	0.043
t_3	1	14	0.01%	12	12	0.94	0.339
w	1	7	0.01%	3	3	0.23	0.635
Square	7	1064	0.74%	1061	152	11.69	0.000
l_1*l_1	1	42	0.03%	6	6	0.44	0.511
t_1*t_1	1	74	0.05%	9	9	0.70	0.409
l_2*l_2	1	924	0.64%	421	421	32.44	0.000
t_2*t_2	1	2	0.00%	0	0	0.00	0.997
l_3*l_3	1	11	0.01%	8	8	0.65	0.424
t_3*t_3	1	11	0.01%	5	5	0.36	0.551
$w*w$	1	0	0.00%	0	0	0.04	0.849
2-Way Interaction	21	240	0.17%	240	11	0.88	0.614
l_1*t1	1	4	0.00%	5	5	0.35	0.555
l_1*l_2	1	0	0.00%	0	0	0.02	0.902
l_1*t_2	1	1	0.00%	1	1	0.11	0.745
l_1*l_3	1	16	0.01%	16	16	1.21	0.277
l_1*t_3	1	1	0.00%	1	1	0.10	0.748
l_1*w	1	2	0.00%	2	2	0.17	0.682
t_1*l_2	1	38	0.03%	33	33	2.54	0.118
t_1*t_2	1	3	0.00%	3	3	0.23	0.635
t_1*l_3	1	0	0.00%	1	1	0.05	0.820
t_1*t_3	1	1	0.00%	1	1	0.07	0.795
t_1*w	1	0	0.00%	0	0	0.00	0.990
l_2*t_2	1	139	0.10%	138	138	10.63	0.002
l_2*l_3	1	5	0.00%	5	5	0.39	0.534
l_2*t_3	1	16	0.01%	16	16	1.26	0.269
l_2*w	1	1	0.00%	1	1	0.04	0.837
t_2*l_3	1	5	0.00%	5	5	0.42	0.520
t_2*t_3	1	0	0.00%	0	0	0.00	0.964
t_2*w	1	3	0.00%	2	2	0.19	0.663
l_3*t_3	1	1	0.00%	1	1	0.11	0.743
l_3*w	1	2	0.00%	2	2	0.13	0.722
t_3*w	1	0	0.00%	0	0	0.03	0.855
Error	43	558	0.39%	558	13		
Total	78	144379	100.00%				

suggestions, the results showed that this hybrid optimization could be effective only if the range of two quality responses was limited well. It was mainly dependent on the designer's experiences. To suppress this dependence, there was two common rules as follows:

(i) The larger-the better objective function: the range of this function should not exceed an allowable value. For example, the maximum displacement of LCM was desired to be about 400 μm, and therefore the range of this response was controlled in the range of 400 μm, as seen in Table 8.

(ii) A minimum high safety was also required, and this function was constrained to be 3, as seen in Table 8.

The history charts of displacement, stress, and safety factor were retrieved from the results of the proposed hybrid optimization algorithm. As seen in Figure 8, the displacement was convergent in the range from 390 μm to 420 μm.

Table 7: Response surface regression of safety factor versus design parameters.

Source	DF	Seq SS	Contribution	Adj SS	Adj MS	F-Value	P-Value
Model	35	10.3266	91.71%	10.3266	0.29505	13.59	0.000
Linear	7	6.2102	55.15%	4.2000	0.60000	27.63	0.000
l_1	1	0.0040	0.04%	0.0070	0.00698	0.32	0.574
t_1	1	0.0033	0.03%	0.0198	0.01980	0.91	0.345
l_2	1	5.6464	50.14%	3.8575	3.85746	177.66	0.000
t_2	1	0.0019	0.02%	0.0195	0.01955	0.90	0.348
l_3	1	0.0062	0.05%	0.0002	0.00015	0.01	0.934
t_3	1	0.0237	0.21%	0.0132	0.01323	0.61	0.439
w	1	0.5248	4.66%	0.3058	0.30581	14.08	0.001
Square	7	3.6100	32.06%	3.6212	0.51731	23.82	0.000
l_1*l_1	1	0.1209	1.07%	0.0723	0.07234	3.33	0.075
t_1*t_1	1	0.1764	1.57%	0.0812	0.08121	3.74	0.060
l_2*l_2	1	3.2129	28.53%	1.1001	1.10007	50.66	0.000
t_2*t_2	1	0.0127	0.11%	0.0783	0.07827	3.60	0.064
l_3*l_3	1	0.0418	0.37%	0.0967	0.09670	4.45	0.041
t_3*t_3	1	0.0105	0.09%	0.0434	0.04343	2.00	0.164
$w*w$	1	0.0348	0.31%	0.0408	0.04083	1.88	0.177
2-Way Interaction	21	0.5064	4.50%	0.5064	0.02411	1.11	0.374
l_1*t1	1	0.0023	0.02%	0.0029	0.00294	0.14	0.715
l_1*l_2	1	0.0010	0.01%	0.0010	0.00104	0.05	0.828
l_1*t_2	1	0.0054	0.05%	0.0053	0.00527	0.24	0.625
l_1*l_3	1	0.0051	0.05%	0.0047	0.00475	0.22	0.642
l_1*t_3	1	0.0010	0.01%	0.0009	0.00092	0.04	0.837
l_1*w	1	0.0016	0.01%	0.0016	0.00165	0.08	0.784
t_1*l_2	1	0.0320	0.28%	0.0306	0.03061	1.41	0.242
t_1*t_2	1	0.0079	0.07%	0.0073	0.00729	0.34	0.565
t_1*l_3	1	0.0000	0.00%	0.0001	0.00008	0.00	0.953
t_1*t_3	1	0.0015	0.01%	0.0016	0.00163	0.08	0.785
t_1*w	1	0.0265	0.24%	0.0246	0.02464	1.13	0.293
l_2*t_2	1	0.1314	1.17%	0.1296	0.12961	5.97	0.019
l_2*l_3	1	0.0041	0.04%	0.0043	0.00433	0.20	0.657
l_2*t_3	1	0.0003	0.00%	0.0002	0.00022	0.01	0.920
l_2*w	1	0.2419	2.15%	0.2428	0.24277	11.18	0.002
t_2*l_3	1	0.0105	0.09%	0.0107	0.01069	0.49	0.487
t_2*t_3	1	0.0058	0.05%	0.0058	0.00580	0.27	0.608
t_2*w	1	0.0045	0.04%	0.0040	0.00402	0.18	0.669
l_3*t_3	1	0.0001	0.00%	0.0001	0.00006	0.00	0.959
l_3*w	1	0.0233	0.21%	0.0233	0.02333	1.07	0.306
t_3*w	1	0.0002	0.00%	0.0002	0.00022	0.01	0.921
Error	43	0.9337	8.29%	0.9337	0.02171		
Total	78	11.2603	100.00%				

Table 8: Bounds of the quality responses.

Characteristics	Constraint type	Lower	Upper	Unit
Maximum displacement	Lower <= Values <= Upper	N/A	400	μm
Minimum safety factor	Values >= Lower	N/A	3	

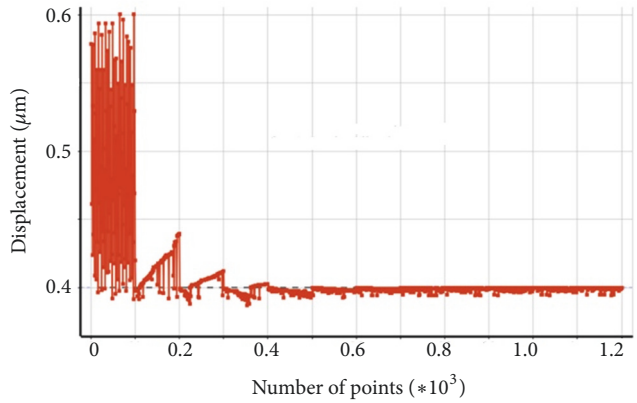

Figure 8: History chart of the displacement.

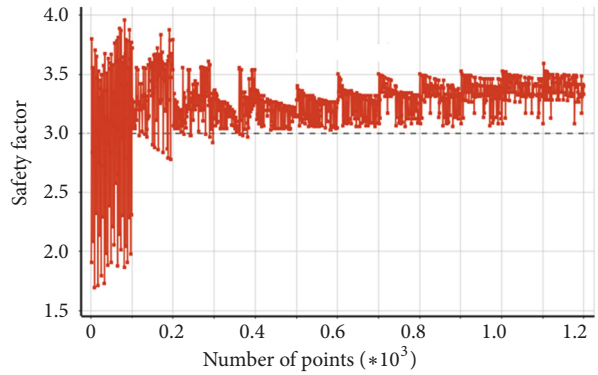

Figure 9: History chart of the safety factor.

Meanwhile, the safety factor was convergent in the range from 3 to 3.5, as shown in Figure 9. It means that the optimal results can be found in the range of desired space. As can be seen in these figures, the curves may be so noisy. It is true that there were so many data points occurring at the optimum space and the optimal cost functions were found in the ranges. Hence, they could be very noisy. This was a new approach compared with previous studies where there was only a convergent solution. The convergence in a range allowed the choice the best solution suitable for a real-work problem.

The pseudo- or virtual mathematical models were found by using ANN approach. To achieve the optimal results for the LCM, the constraints for two objective functions were set up, as given in Table 5. Three potential candidates were generated. As given in Table 9, the potentially optimal design parameters were found with similar values for each factor. How to choose the best candidate was dependent on user's requirements.

Before selecting the best optimal solution for the LCM, the best tuning parameters of MOGA algorithm were selected. As given in Table 2, the tuning parameters for MOGA were set in this study as follows: the population size is within the range of 20-100, the crossover probability is within the range of 0.2-0.90, the mutation probability is within the range of 0.01-0.02, and the number of generation is within the range of 50-150. To find the best parameters for the MOGA, after thirty times of computational simulations, the best parameters of MOGA were chosen as follows: population size of 100, crossover probability of 0.7, mutation probability of 0.01, and number of generation of 100.

A shown in Table 10, candidate 1 was chosen as the best optimal design because it fully satisfies the mentioned design objectives and the resulting stress of 140.6496 MPa was lowest and highest safety factor of 3.5952. The minimum stress could guarantee a fatigue life and long working time. The predicted results indicated that the optimal results were found at the displacement of 398.5 μm, a minimal stress of 140.65 MPa, and safety factor of 3.6.

The Pareto-optimal fronts and results obtained from the MOGA algorithm were than compared to those obtained using the Elitist Nondominated Sorting Genetic Algorithm (NSGA-II) [28]. Common parameters for NSGA-II are included: the population size is within the range of 20-100, the crossover probability is within the range of 0.2-0.9, the mutation probability is within the range of 0.1-0.2, and the number of generation is within the range of 50-150.

A basic way to find good parameters for the algorithm is preliminary runs. After thirty times of computational simulations, the best parameters of NSGA-II were chosen as follows: population size of 75, crossover probability of 0.8, mutation probability of 0.2, and number of generation of 110. The

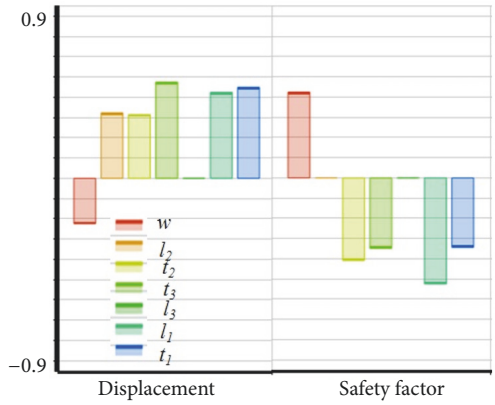

Figure 10: Sensitivity diagram.

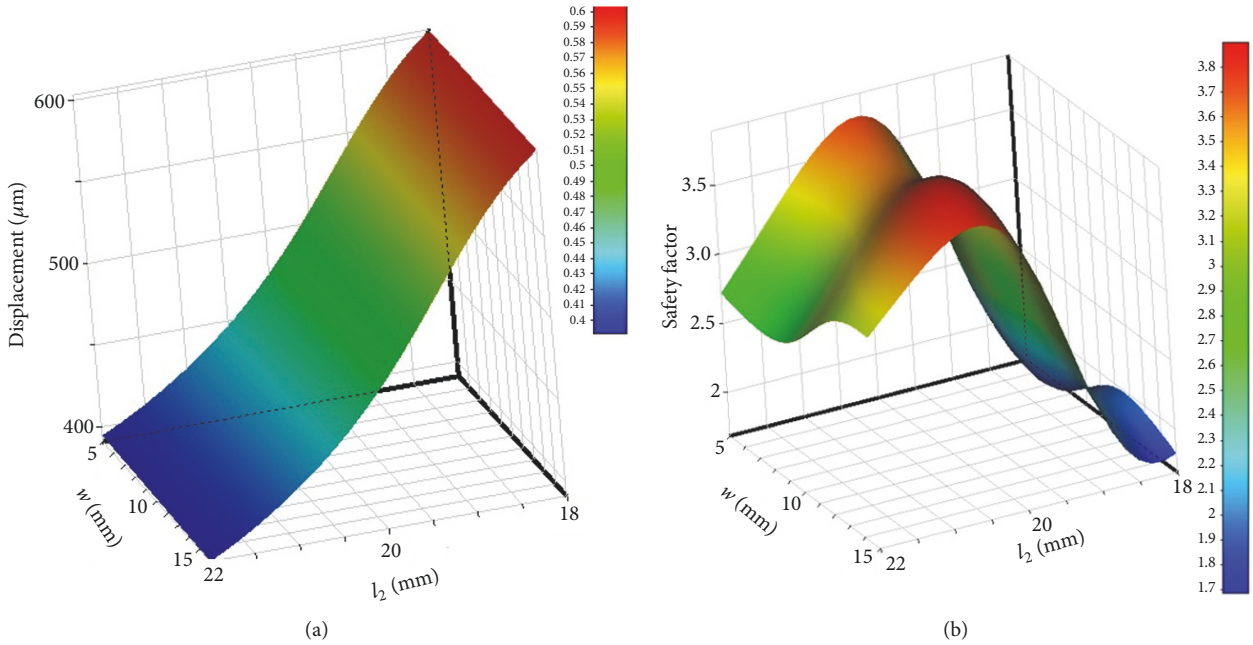

Figure 11: Effect diagram of w and l_2 on (a) the displacement and (b) safety factor.

Table 9: Potentially optimal design parameters.

Candidates	l_1 (mm)	t_1 (mm)	l_2 (mm)	t_2 (mm)	l_3 (mm)	t_3 (mm)	w (mm)
Candidate 1	27.04	0.46	21.45	0.38	5.73	0.45	14.23
Candidate 2	28.48	0.45	21.79	0.36	6.57	0.52	14.32
Candidate 3	29.94	0.46	21.81	0.37	6.56	0.53	14.39

Table 10: Comparison among potentially optimal performances.

Performances	Candidate Point 1	Candidate Point 2	Candidate Point 3
Equivalent stress (MPa)	140.6496	150.1017	155.1464
Displacement (μm)	398.5	399.8	399.7
Safety factor	3.5952	3.5285	3.4986

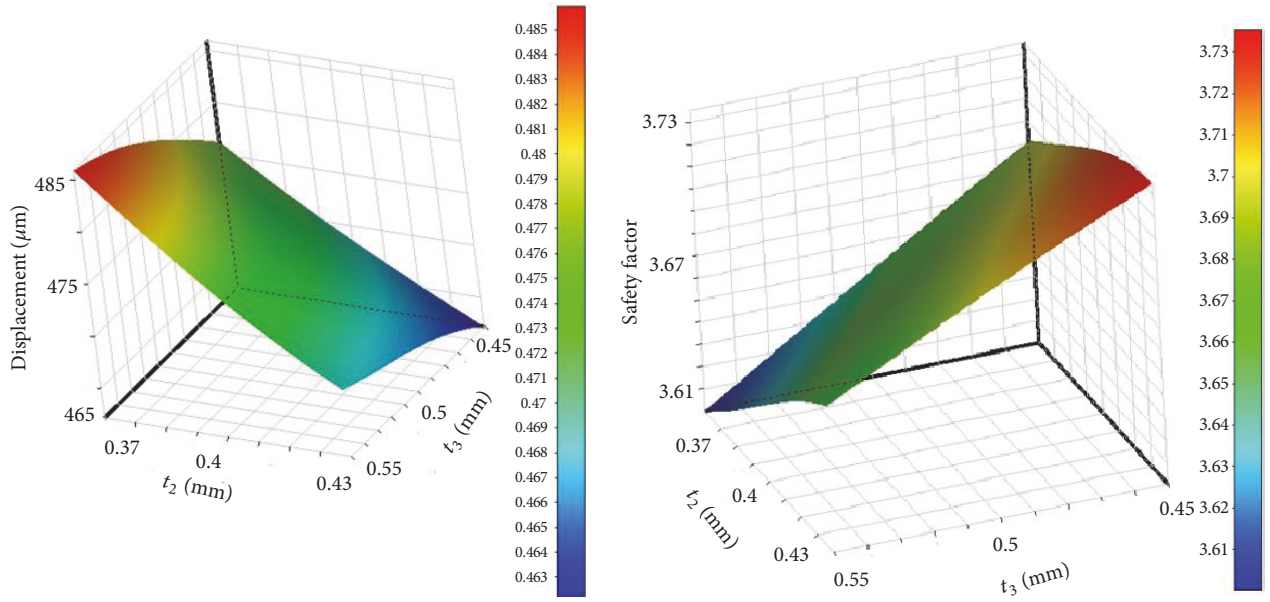

(a) (b)

Figure 12: Effect diagram of t_2 and t_3 on (a) the displacement and (b) safety factor.

Table 11: Comparison of the optimal performances obtained from MOGA an NSGA-II.

Performances	MOGA	NSGA-II
Equivalent stress (MPa)	140.65	140.82
Displacement (μm)	398.5	397.4
Safety factor	3.60	3.57
Computational time (minute)	9.7	10.5

comparative results showed that the optimal performances from the MOGA are better than those obtained from the NSGA-II. Specifically, the stress from MOGA was smaller than that from NSGA-II, and the displacement and safety factor from MOGA were higher than those from NSGA-II. Besides, the computational optimization time required for MOGA was less than that for NSGA-II, as given in Table 11.

5.5. Statistical Analysis. In order to evaluate the behavior of the evolutionary algorithms, a statistical analysis is often used. In this study, the Wilcoxon's rank signed test was applied to describe the behavior of the MOGA. It was a statistically nonparametric technique applied for various fields [29, 30]. For details about this procedure, the readers can refer to [29, 30]. To investigate the behavior of the MOGA, the NSGA-II was used simultaneously to make the two algorithm pairs. A comparison of two algorithms aimed to discover the significant difference between their behaviors. The computational simulations were conducted with 30 runs for each algorithm. The Wilcoxon's rank signed test was performed at 5% significant level. The results of Wilcoxon's rank signed test were given in Table 12. It showed three parameters, namely, R-, R+, and p-value. The MOGA showed significantly better results than the NSGA-II with p-value of 0.006.

Table 12: The results of Wilcoxon's rank signed test.

Pair	R-	R+	p-value
MOGA-NSGA-II	-0.2	0	0.006

5.6. Analysis of Sensitivity. Along with optimization process, a sensitivity analysis is also a necessary step to determine an influence of each design parameter on each quality response. For the proposed LCM, the sensitivity analysis was mainly focused on three characteristics. Generally, there were many methods that can be applied for calculating the sensitivity such as Nelson method, modal method, matrix perturbation method, differential method, RSM, or statistical analysis [31, 32]. For example, the direct differential method takes more time for analysis because it needs to construct physical models. Therefore, RSM was chosen for this study. The sensitivity could be calculated by following formula:

$$S_f = \frac{\partial f_i}{\partial x_i}, \tag{16}$$

where f_i, x are the quality response and the design parameter ith, respectively.

In this study, seven variables and two quality characteristics were considered. As seen in Figure 10, regarding

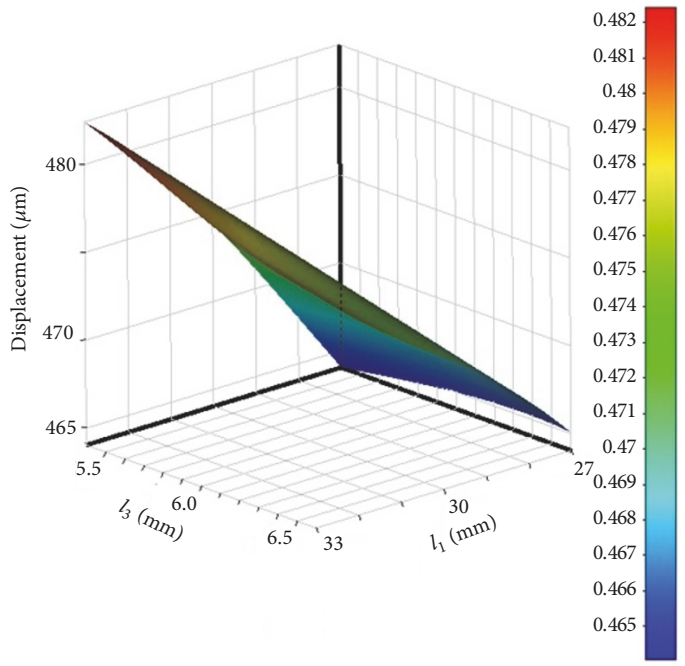

(a)

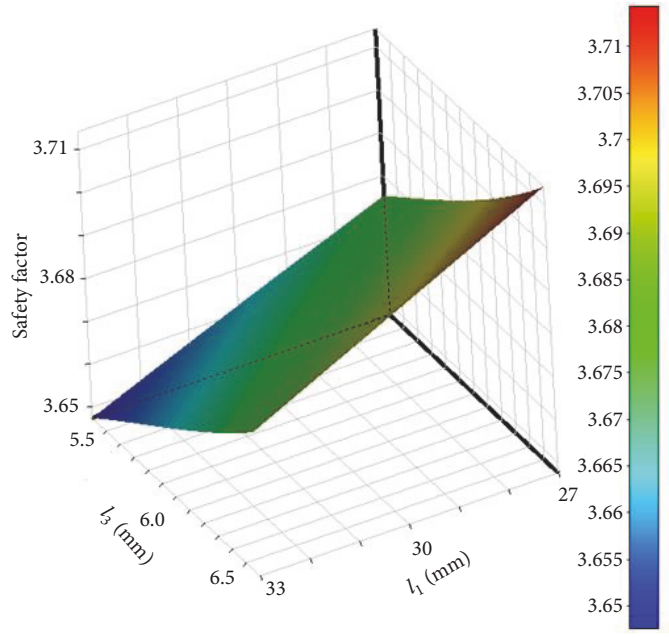

(b)

Figure 13: Effect diagram of l_1 and l_3 on (a) the displacement and (b) safety factor.

the displacement's sensitivity, thickness t_3 had a highest influence or significant contribution on the displacement while the length l_3 had a lowest contribution. It was noted that a change in t_3 would adjust the displacement as desired. Other parameters were in relatively middle effects. Regarding the safety factor, the lengths l_2 and l_3 had the smallest contributions while the length l_1 had the largest effect on the safety factor. To adjust the safety factor, the l_1 should be changed firstly.

Particularly, Figure 11(a) illustrates the effects of the width w and length l_2 on the displacement. The results indicated that the displacement has a linear change corresponding to the width while it has a nonlinear influence with respect to the length. Figure 11(b) shows the effects of the width w

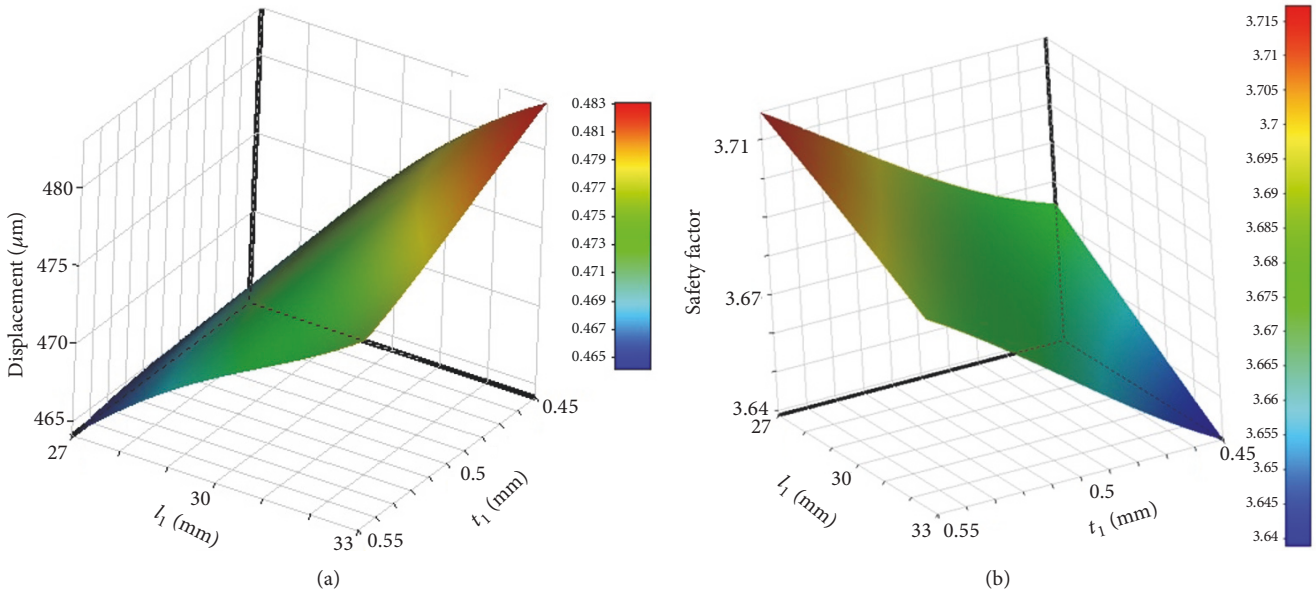

Figure 14: Effect diagram of l_1 and t_1 on (a) the displacement and (b) safety factor.

and length l_2 on the safety factor. The results indicated that the safety factor has a nonlinear effect corresponding to the width and it also has a nonlinear influence with respect to the length. In particular, the length had a more significant contribution to the safety factor compared with the width because this response was changed sharply. An increase in the length made a decrease in the safety factor.

The contribution diagrams of thicknesses t_2 and t_3 were plotted in Figures 12(a) and 12(b), respectively. The results revealed that both parameters almost have a nonlinear influence on the displacement. When the thickness was increased, this response was lowered, as seen in Figure 10(a). Meanwhile, both design variables had a relatively linear contribution on this response. It means that the safety factor was linearly raised with respect to these parameters, as given in Figure 12(b).

As depicted in Figure 13(a), the lengths l_1 and l_3 had a nearly linear influence with the displacement but they had a nonlinear contribution affecting the safety factor.

As seen in Figure 14(a), the thickness t_1 had a nonlinear influence on the displacement as well as the safety factor.

Summary, almost the mentioned design parameters had significant contributions to the displacement and safety factor. This would help designers and researchers to make a decision and meet the requirements of a specific system.

6. Verifications

To evaluate and validate the optimal performances of the proposed LCM, simulation tests were carried out. Using the optimal design variables of candidate 1 in Table 6, the prototype of LCM was created. Extra experimental validations were conducted and the average value was retrieved.

As given in Table 13, the results indicated that the optimal results were found at the displacement of 398.5 μm and safety factor of 3.5952. The results found that the predicted and experimental results are in a good agreement. It means that the proposed hybrid optimization method is actually robust approach to solve multiobjective optimization problem for the LCM. It can be applied to solve complex optimization problems. Compared with the initial design, the displacement and safety factor were improved by about 2.5% and 4.7%, respectively, as shown in Table 14.

7. Conclusions

This paper presented a new intelligent evolutionary multiobjective optimization approach for a linear compliant mechanism. The mechanism was designed based on connecting series of the leaf springs. These springs were located in symmetric configuration not only to guarantee a motion linearity but also to increase the working travel. To improve overall static performances, including the large working travel and high safety factor, a hybrid optimization approach was developed. This approach was an integration of FEM, RSM, ANN method, and MOGA. Three optimal candidates were retrieved and then candidate 1 was chosen as the finally optimum solution.

The sensitivity analysis was carried out to determine the significant contribution of each factor. The results revealed that the lengths and thickness are main influencers. The results revealed that the lengths and thickness almost significantly affect both responses. The results showed that the optimal results were found at the displacement of 330.68 μm, stress of 140.6496 MPa, and safety factor of 3.5952. The predicted results were highly consistent with the experimental results. It was confirmed that the proposed hybrid optimization approach is highly robust to solve complex optimization engineering problems.

Table 13: Competition predicted and experimental results.

Characteristics	Prediction	Experiment	Error (%)
Displacement (μm)	330.68	326.0174	1.43
Stress (MPa)	140.6496	139.4822	0.83
Safety factor	3.5952	3.5872	0.22

Table 14: Comparison of initial design with optimal design.

Responses	Initial design	Optimal design	Improvement (%)
Displacement (μm)	295.59	330.68	11.87
Safety factor	2.7331	3.5952	31.54

Data Availability

The data used to support the findings of this study are included within the article.

Conflicts of Interest

The authors declare that there are no conflicts of interest regarding the publication of this article.

Acknowledgments

This research is funded by Vietnam National Foundation for Science and Technology Development (NAFOSTED) under grant number 107.01-2016.20.

References

[1] W. O'Brien, "Long-range motion with nanometer precision," *Photonics Spectra*, vol. 39, no. 6, pp. 80-81, 2005.

[2] S. Polit and J. Dong, "Development of a high-bandwidth XY nanopositioning stage for high-rate micro-/nanomanufacturing," *IEEE/ASME Transactions on Mechatronics*, vol. 16, no. 4, pp. 724–733, 2011.

[3] M.-G. Song, H.-W. Baek, N.-C. Park et al., "Development of small sized actuator with compliant mechanism for optical image stabilization," *IEEE Transactions on Magnetics*, vol. 46, no. 6, pp. 2369–2372, 2010.

[4] T.-P. Dao and S.-C. Huang, "Compliant thin-walled joint based on zygoptera nonlinear geometry," *Journal of Mechanical Science and Technology*, vol. 31, no. 3, pp. 1293–1303, 2017.

[5] R. F. Fung, Y. L. Hsu, and M. S. Huang, "System identification of a dual-stage XY precision positioning table," *Precision Engineering*, vol. 33, no. 1, pp. 71–80, 2009.

[6] T.-P. Dao and S.-C. Huang, "Design and multi-objective optimization for a broad self-amplified 2-DOF monolithic mechanism," *Sādhanā*, vol. 42, no. 9, pp. 1527–1542, 2017.

[7] S.-C. Huang and T.-P. Dao, "Design and computational optimization of a flexure-based XY positioning platform using FEA-based response surface methodology," *International Journal of Precision Engineering and Manufacturing*, vol. 17, no. 8, pp. 1035–1048, 2016.

[8] S.-C. Huang and T.-P. Dao, "Multi-objective optimal design of a 2-DOF flexure-based mechanism using hybrid approach of Grey-Taguchi coupled response surface methodology and entropy measurement," *Arabian Journal for Science and Engineering*, vol. 41, no. 12, pp. 5215–5231, 2016.

[9] E. Burman, D. Elfverson, P. Hansbo, M. G. Larson, and K. Larsson, "Shape optimization using the cut finite element method," *Computer Methods Applied Mechanics and Engineering*, vol. 328, pp. 242–261, 2018.

[10] S. Baugreet, J. P. Kerry, A. Brodkorb et al., "Optimisation of plant protein and transglutaminase content in novel beef restructured steaks for older adults by central composite design," *Meat Science*, vol. 142, pp. 65–77, 2018.

[11] A. R. Fares, A. N. Elmeshad, and M. A. A. Kassem, "Enhancement of dissolution and oral bioavailability of lacidipine via pluronic P123/F127 mixed polymeric micelles: Formulation, optimization using central composite design and in vivo bioavailability study," *Drug Delivery*, vol. 25, no. 1, pp. 132–142, 2018.

[12] S. Mosleh, M. R. Rahimi, M. Ghaedi, K. Dashtian, and S. Hajati, "Sonochemical-assisted synthesis of CuO/Cu2O/Cu nanoparticles as efficient photocatalyst for simultaneous degradation of pollutant dyes in rotating packed bed reactor: LED illumination and central composite design optimization," *Ultrasonics Sonochemistry*, vol. 40, pp. 601–610, 2018.

[13] F. Nemati, R. Zare-Dorabei, M. Hosseini, and M. R. Ganjali, "Fluorescence turn-on sensing of thiamine based on Arginine – functionalized graphene quantum dots (Arg-GQDs): Central composite design for process optimization," *Sensors and Actuators B: Chemical*, vol. 255, pp. 2078–2085, 2018.

[14] A. Raheem, G. Ji, A. Memon et al., "Catalytic gasification of algal biomass for hydrogen-rich gas production: Parametric optimization via central composite design," *Energy Conversion and Management*, vol. 158, pp. 235–245, 2018.

[15] S. Shariati, E. Bozorgzadeh, F. Shariati, and F. Safa, "Ionic Liquid Based Ultrasound-Assisted Emulsification Microextraction for Preconcentration of Phenol Using Central Composite Design," *Journal of Analytical Chemistry*, vol. 73, no. 1, pp. 36–41, 2018.

[16] A. Albanesi, F. Bre, V. Fachinotti, and C. Gebhardt, "Simultaneous ply-order, ply-number and ply-drop optimization of laminate wind turbine blades using the inverse finite element method," *Composite Structures*, vol. 184, pp. 894–903, 2018.

[17] A. Karamanlı and T. P. Vo, "Size dependent bending analysis of two directional functionally graded microbeams via a quasi-3D theory and finite element method," *Composites Part B: Engineering*, vol. 144, pp. 171–183, 2018.

[18] N. Le Chau, V. A. Dang, H. G. Le, and T.-P. Dao, "Robust Parameter Design and Analysis of a Leaf Compliant Joint for Micropositioning Systems," *Arabian Journal for Science and Engineering*, vol. 42, no. 11, pp. 4811–4823, 2017.

[19] T. Zhang, Z. Chen, J. Liu, and X. Li, "The artificial neural networks based on scalarization method for a class of bilevel biobjective programming problem," *Comput Intell Neurosci*, vol. 2017, Article ID 1853131, 14 pages, 2017.

[20] A. Zamaniyan, F. Joda, A. Behroozsarand, and H. Ebrahimi, "Application of artificial neural networks (ANN) for modeling of industrial hydrogen plant," *International Journal of Hydrogen Energy*, vol. 38, no. 15, pp. 6289–6297, 2013.

[21] Vijay G. S., Kumar H. S., Srinivasa Pai P., Sriram N. S., and R. B. Rao, "Evaluation of Effectiveness of Wavelet Based Denoising Schemes Using ANN and SVM for Bearing Condition Classification," *Computational Intelligence and Neuroscience*, vol. 2012, Article ID 582453, 12 pages, 2012.

[22] B. A. Garro and R. A. Vázquez, "Designing artificial neural networks using particle swarm optimization algorithms," *Computational Intelligence and Neuroscience*, vol. 2015, Article ID 369298, 20 pages, 2015.

[23] M. Hemmat Esfe, S. Esfandeh, S. Saedodin, and H. Rostamian, "Experimental evaluation, sensitivity analyzation and ANN modeling of thermal conductivity of ZnO-MWCNT/EG-water hybrid nanofluid for engineering applications," *Applied Thermal Engineering*, vol. 125, pp. 673–685, 2017.

[24] S. H. Mousavi-Avval, S. Rafiee, M. Sharifi et al., "Application of multi-objective genetic algorithms for optimization of energy, economics and environmental life cycle assessment in oilseed production," *Journal of Cleaner Production*, vol. 140, pp. 804–815, 2017.

[25] S. Wang, G. Jian, J. Wang, L. Sun, and J. Wen, "Application of entransy-dissipation-based thermal resistance for performance optimization of spiral-wound heat exchanger," *International Journal of Heat and Mass Transfer*, vol. 116, pp. 743–750, 2018.

[26] J. Wen, X. Gu, M. Wang, S. Wang, and J. Tu, "Numerical investigation on the multi-objective optimization of a shell-and-tube heat exchanger with helical baffles," *International Communications in Heat and Mass Transfer*, vol. 89, pp. 91–97, 2017.

[27] T.-P. Dao, "Multiresponse optimization of a compliant guiding mechanism using hybrid taguchi-grey based fuzzy logic approach," *Mathematical Problems in Engineering*, vol. 2016, 17 pages, 2016.

[28] K. Deb, S. Agrawal, A. Pratap, and T. Meyarivan, "A fast elitist non-dominated sorting genetic algorithm for multi-objective optimization: NSGA-II," *Lecture Notes in Computer Science*, vol. 1917, pp. 849–858, 2000.

[29] E. Cuevas, J. Gálvez, S. Hinojosa, O. Avalos, D. Zaldívar, and M. Pérez-Cisneros, "A comparison of evolutionary computation techniques for IIR model identification," *Journal of Applied Mathematics*, vol. 2014, 2014.

[30] S. García, D. Molina, M. Lozano, and F. Herrera, "A study on the use of non-parametric tests for analyzing the evolutionary algorithms' behaviour: a case study on the CEC'2005 Special Session on Real Parameter Optimization," *Journal of Heuristics*, vol. 15, no. 6, pp. 617–644, 2009.

[31] N. L. Chau, T. Dao, and V. T. Nguyen, "Optimal Design of a Dragonfly-Inspired Compliant Joint for Camera Positioning System of Nanoindentation Tester Based on a Hybrid Integration of Jaya-ANFIS," *Mathematical Problems in Engineering*, vol. 2018, pp. 1–16, 2018.

[32] N. L. Ho, T. Dao, H. G. Le, and N. L. Chau, "Optimal Design of a Compliant Microgripper for Assemble System of Cell Phone Vibration Motor Using a Hybrid Approach of ANFIS and Jaya," *Arabian Journal for Science and Engineering*, pp. 1–16, 2018.